Metallic phase of disordered graphene superlattices with long-range correlations

Hosein Cheraghchi,[1,*] Amir Hossein Irani,[1] Seyed Mahdi Fazeli,[2] and Reza Asgari[3,†]
[1]*School of Physics, Damghan University, 6715-364 Damghan, Iran*
[2]*Physics Department, University of Qom, Qom, Iran*
[3]*School of Physics, Institute for Research in Fundamental Sciences, IPM 19395-5531 Tehran, Iran*
(Received 4 October 2010; revised manuscript received 8 April 2011; published 29 June 2011)

Using the transfer-matrix method, we study the conductance of chiral particles through a monolayer graphene superlattice with long-range correlated disorder distributed on the potential of the barriers. Even though the transmission of the particles through a graphene superlattice with white-noise potentials is suppressed, the transmission is revived in a wide range of angles when the potential heights are long-range correlated with a power spectrum $S(k) \sim 1/k^{\beta}$. As a result, the conductance increases with increasing correlation-exponent values giving rise to a metallic phase. We obtain a phase-transition diagram in which the critical correlation exponent depends strongly on the disorder strength and slightly on the energy of the incident particles. The phase transition, on the other hand, appears in all ranges of the energy from propagating to evanescent mode regimes.

DOI: 10.1103/PhysRevB.83.235430 PACS number(s): 72.80.Vp, 73.22.Pr, 73.23.−b, 73.63.−b

I. INTRODUCTION

The exploration of graphene, a monolayer of carbon atoms tightly packed into a honeycomb lattice, has recently attracted special attention in the investigation of fundamental physics and also probable device applications such as nanoelectronic devices based on planar graphene structures.[1,2] In graphene, due to its unique band structure with the valence and conduction bands touching at two inequivalent Dirac points, electrons around the Fermi level obey the massless relativistic Dirac equation, which results in a linear energy-dispersion relation.[3] Massless relativistic quasiparticles arising from the cone spectrum lead to a number of unusual electronic properties such as anomalous integer[4] and fractional[5] quantum Hall effects, focusing of electrons by a rectangular potential barrier (so-called Veselago lensing),[6] special Andreev reflection,[7] and observation of the plasmaron composite[8] and minimal conductivity.[9]

Interestingly, relativistic quantum quasiparticles incident normally to a high electrostatic potential barrier in graphene can pass through it with perfect transmission regardless of the height or width of the barrier.[10] This phenomenon, which is referred to as the Klein tunneling, is in contrast with the quantum massive-carrier tunneling, where the transmission probability decays exponentially with increasing barrier height and width. Recently, evidence for the Klein tunneling of the Dirac fermions across a p-n junction have been experimentally observed when a gate-induced potential step has been steep enough.[11,12]

In graphene sheets, the type of particles (electrons or holes) and the density of the carriers can be controlled by tuning a gate bias voltage.[13–15] Moreover, graphene superlattices may be fabricated by adsorbing adatoms on the graphene surface, by positioning and aligning impurities with scanning tunneling microscopy,[16] or by applying a local top gate voltage to graphene.[17] The transmission of hitting massless particles in a clean[18] or disordered[19] graphene-based superlattice structure has been studied. It was shown that the conductivity of the system depends on the superlattice structural parameters.

The first study on electronic properties of monolayer and bilayer graphene superlattices was performed by Bai and Zhang.[18] They showed that the angular-averaged conductivity can be controlled by changing the structure parameters. Furthermore, it has been also shown that massless Dirac fermions are generated in an one-dimensional external periodic potential close to the original Dirac point.[20,21] The Dirac points depend on system parameters, for instance, the potential of the barriers/wells and the period of the potential and transverse wave number.[22] An evidence for such Dirac points is the conductance resonances that appear at special potential values.[21] Moreover, the conductance of a graphene superlattice with uncorrelated disorder in the width of the barriers was calculated in Ref. 19. It was shown that the transmission of the quasiparticles with large angles of incidence to the potential barriers is suppressed by disorder strength and the sample size too. Therefore, the results of the finite-size-scaling computations predicted a zero conductance for all the graphene superlattices, except for some resonant barrier thickness for which the conductance tends to a nonzero constant in the thermodynamic limit.[19]

A number of numerical calculations of electron transport confirmed the absence of localization in the presence of a long-range random potential in disordered graphene.[23] The main quantity that is mostly studied numerically is the conductance, G, of a finite-size graphene sample with a width, W, much larger than the length, L. The setup allows us to define the "conductivity" $\sigma = GL/W$ even for ballistic samples with L much shorter than the mean free path, l.

It is well known that the transmission of quantum massive carriers unexpectedly increases when special correlation is applied on disorder.[24] This is in contrast with the Anderson localization in which all states are exponentially localized in one-dimensional uncorrelated disorder. Experimental evidence for a discrete number of extended states has been observed in random-dimer semiconductor superlattices as a short-range correlated disorder.[25] Long-range correlated sequences of the potential barriers in semiconductor superlattices, however, could result in a continuum of extended states giving rise to mobility edges.[26–28] Application of a long-range correlated random sequence on the length of some screws was used to model scatterers in a single-mode wave guide.[29] By applying

appropriate correlations between scatterers, it was shown that the microwave transmission spectra displays a transparent frequency interval that is separated by a mobility edge from the nontransparent frequency intervals.

In this paper, we study the conductance of massless Dirac fermions through graphene superlattices with a long-range correlated disorder on the potentials of the barriers. Application of disorder on the potentials of the barriers could be experimentally manifested by coating some top gate voltages on the graphene sheet.[29] The transmission of the large-angles incident electrons to the graphene superlattice, which is suppressed by uncorrelated disorder, is revived by applying correlation between the random potentials of the barriers. As a result, the conductance increases with the correlation exponent. Consequently, an insulator-to-metal transition emerges at a critical correlation exponent that depends strongly on the disorder strength. One should notice that such a phase transition emerges for the entire range of energies. In addition, the dependence of the conductance on the superlattice parameters is investigated for different correlation strengths.

The paper is organized as follows. We present the transfer-matrix and Fourier-filtering methods used to calculate the transmission through the long-range correlated graphene superlattices in Sec. II. Our results and related discussion will be presented in Sec. III where we also present the metal-to-insulator phase transition and investigate the emergence of the phase transition along different energy ranges. The conclusions are given in last section.

II. MODEL AND THE TRANSFER MATRIX

In the low-energy limit, charge carriers near the Dirac point in the continuum model can be described by the following noninteracting Hamiltonian:

$$\mathcal{H} = -i\hbar v_F(\sigma_x \partial_x + \sigma_y \partial_y) + V(x), \tag{1}$$

where $v_F = 10^6$ m/s is the Fermi velocity and σ_x and σ_y are the Pauli matrices. We consider a lattice of electrostatic potentials as barriers that are induced by top gate voltages. Therefore, the potentials of the barriers are sorted as follows:

$$V(x) = \begin{cases} V_i & d_{2i-1} < x < d_{2i}, \quad i = 1,2,\ldots, \\ 0 & \text{elsewhere.} \end{cases} \tag{2}$$

A schematic representation of our graphene superlattice is shown in Fig. 1. We consider the number of regions (wells and barriers) to be equal to N and that there are $(N-1)/2$ barriers. The widths of the barriers and wells are considered to be fixed. The height of the barriers fluctuates around its mean and is defined by $V_i = \langle V \rangle (1 + \sigma \varepsilon_i)$, where σ is the variance of the potentials of the barriers and $\{\varepsilon_i\}$ is a long-range correlated random sequence of data with the Gaussian distribution.

Before calculating the conductance, we might sometimes generate a random sequence with a long-range correlation. A correlated sequence $\{\varepsilon_i\}$ will be considered to describe the trace of a fractional Brownian motion with a power spectrum $S(k) \sim 1/k^\beta$, where $1 < \beta < 3$ and $\beta = 2H + 1 = 2\alpha - 1$ $(1 < \alpha < 2)$. Here H is the Hurst exponent. In the case of

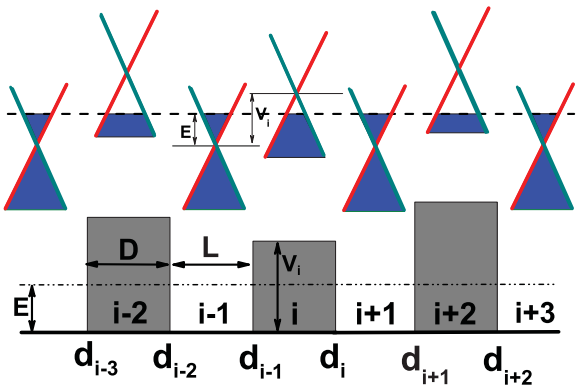

FIG. 1. (Color online) Graphene superlattice with long-range correlated disorder on the potential barriers.

power-law decaying autocorrelations, the correlation function decays with an exponent γ such that $C(x_i - x_j) \propto |i-j|^{-\gamma}$, where $\gamma = 1 - \beta$. Random sequences with weaker positive correlation are generated with $0.5 < \alpha < 1$, which is referred to as the fractional Gaussian noise.[30] In this case, $\beta = 2H - 1 = 2\alpha - 1$ and $\alpha = 0.5$ correspond to uncorrelated disorder or white noise.

It is common to apply a Fourier-filtering method[31] to generate a sequence with a long-range correlation. This method contains the following steps: (i) a sequence of white-noise random numbers $\{\theta_i\}$ with a Gaussian distribution is generated. (ii) The transformation of the Fourier components of $\{\theta_i\}$ is attributed to a sequence that is called $\{\theta_k\}$. (iii) An inverse Fourier transformation of the sequence $\{\varepsilon_k = k^{-\beta/2}\theta_k\}$ results in the sequence of interest, $\{\varepsilon_i\}$. (iv) Finally, the random sequences become normalized, accordingly the mean value, ε_i, is set to be zero and its variance is fixed. Three landscapes of random data generated by the mentioned method are shown in Fig. 2 for different correlation exponents. In Appendix B, the distribution function and also the pair-correlation function of a correlated random sequence generated by the above algorithm is shown in Fig. 13. Clearly, the correlation between

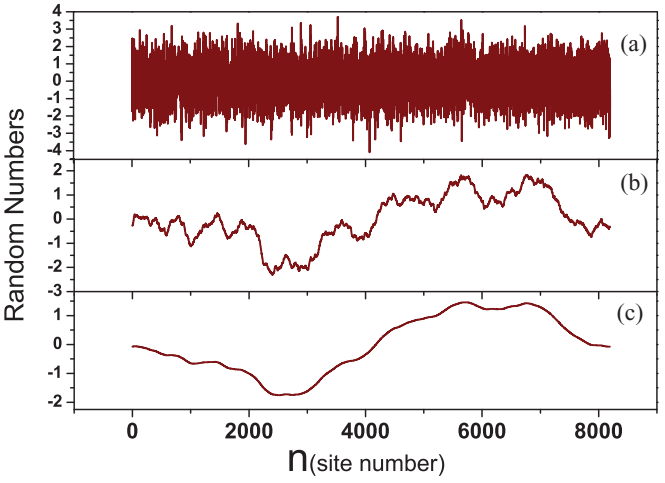

FIG. 2. (Color online) Random distribution of the correlated sequences generated by a Fourier-filtering method. (a) Uncorrelated case corresponding to $\alpha = 0.500$, (b) $\alpha = 1.766$, and (c) $\alpha = 1.993$.

random potentials leads to a reduction in the fluctuations of the random distribution. We should notice that we have checked the invariance of our results in comparison to those results obtained from random sequences produced by the midpoint method.[30]

Having such a configuration of the potentials gives rise to a superlattice that consists of two types of graphene: electron-doped and hole-doped. The doping type of graphene in wells is n-type for quasiparticles with an incident energy $E = \hbar v_F/\lambda > 0$, where λ is the electron wavelength in the wells. The doping type in the barriers depends on the potential height, V_i. In other words, the ith barrier is hole-doped graphene if $E < V_i$, while it is electron-doped if $E > V_i$. Accordingly, the type of doping in the barriers is also altered randomly. We assume that the angle of incidence for electrons is $\phi = \varphi_1$ along the x axis. However, the transfer matrix takes the angle of each region into account separately. The general solution of Eq. (1) results in the following spinor for the ith region:

$$\psi(x,y) = a_i \begin{Bmatrix} 1 \\ s_i e^{i\varphi_i} \end{Bmatrix} e^{i(k_{ix}x + k_y y)} + b_i \begin{Bmatrix} 1 \\ s_i e^{i(\pi-\varphi_i)} \end{Bmatrix} e^{i(-k_{ix}x + k_y y)}, \quad (3)$$

where a_i and b_i are the transmission and reflection amplitudes, respectively. Other parameters in the spinor are

$$s_i = \mathrm{sgn}(E - V_i), \quad k_y = k_F^i \sin(\varphi_i) = k_F^i \sin\phi,$$
$$k_{ix} = \sqrt{\left[\frac{E - V(x)}{\hbar v_F}\right]^2 - k_y^2}, \quad \varphi_i = \arctan(k_y/k_{ix}). \quad (4)$$

If the energy of the incident electrons is close to V_i value in the ith barrier, k_{ix} becomes imaginary for some angles, resulting in an evanescent mode. In disordered graphene superlattice, evanescent modes emerge when $E \simeq \langle V \rangle$. The transfer matrix is extracted by the continuity of the wave functions at the junction interfaces. It can make a relation between the wave functions of two sides of a step potential from the ith region to the $(i+1)$th like

$$\begin{pmatrix} a_{i+1} \\ b_{i+1} \end{pmatrix} = M_{i+1,i} \begin{pmatrix} a_i \\ b_i \end{pmatrix}, \quad (5)$$

where the transfer matrix $M_{i+1,i}$ is

$$M_{i+1,i} = \begin{pmatrix} m_{11} & m_{12} \\ m_{12}^* & m_{11}^* \end{pmatrix} \quad (6)$$

and the matrix elements of M are

$$m_{11} = e^{i[k_{ix} - k_{(i+1)x}]x_i} \left(\frac{s_{i+1} e^{-i\varphi_{i+1}} + s_i e^{i\varphi_i}}{2 s_{i+1} \cos\varphi_{i+1}} \right),$$
$$m_{12} = e^{-i[k_{ix} + k_{(i+1)x}]x_i} \left(\frac{s_{i+1} e^{-i\varphi_{i+1}} - s_i e^{-i\varphi_i}}{2 s_{i+1} \cos\varphi_{i+1}} \right). \quad (7)$$

The current in the x direction and in the ith region can be derived as

$$J_x^i = v_F \psi^\dagger \sigma_x \psi = 2 v_F s_i \cos\varphi_i (|a_i|^2 - |b_i|^2). \quad (8)$$

Current conservation between regions ith and jth implies

$$|a_j|^2 - |b_j|^2 = \mathrm{Det}[M_{j,i}](|a_i|^2 - |b_i|^2), \quad (9)$$

where

$$M_{j,i} = M_{j,j-1} M_{j-1,j-2} \ldots M_{i+1,i}$$
$$\mathrm{Det}[M_{j,i}] = (s_i \cos\varphi_i)/(s_j \cos\varphi_j). \quad (10)$$

The total transfer matrix which makes a relation between incident and transmitted wave functions is a series product of the transfer matrices arising from each interface. For N regions incorporating the barriers and wells, according to Eq. (11), the matrix is defined as $P = M_{N,1}$.

If the first and last regions of the superlattice are electron-doped graphene, the transmission probability for $(N-1)/2$ barriers can be calculated by means of the product matrices for $b_N = 0$ as

$$T(E,\phi) = \frac{J_{\mathrm{out}}^N}{J_{\mathrm{in}}^1} = \frac{1}{\mathrm{Det}[P]} \left| \frac{a_N}{a_1} \right|^2, \quad (11)$$

where J_{out}^N and J_{in}^1 are out- and inflowing currents, respectively. Because the configuration of the potential barriers is considered such that $s_1 = s_N$ and $\varphi_1 = \varphi_N = \phi$, the conservation of the current between the first and last regions implies that $\mathrm{Det}[P] = 1$. Therefore, the transmission formula can be simplified as $T(E,\phi) = 1/|P_{22}|^2$ where $a_N/a_1 = \mathrm{Det}[P]/P_{22}$. Finally, using Landauer-Büttiker formula[32] and an angular averaging, the conductance is obtained by the following integration:

$$G = G_0 \int_{-\pi/2}^{\pi/2} T(E,\phi) \cos(\phi) d\phi, \quad (12)$$

where $G_0 = e^2 m v_F W/\hbar^2$. Here, W is the finite width of graphene ribbon along the y direction.

III. RESULTS AND DISCUSSION

A. Phase transition

Let us first calculate the transmission probability and study the electronic properties of disordered graphene superlattices. The transmission of electrons hitting the disordered graphene superlattice as a function of the incident angle is shown in Fig. 3 for several values of correlation strengths characterized by the correlation exponent α. In all calculations, the barrier and well widths are considered to be $D = 50$ nm and $L = 30$ nm, respectively. Moreover, we assumed that the energy of the charge carriers and the averaged potential of barriers being $E = 50$ meV and $\langle V \rangle = 200$ meV, respectively. The wavelength of the incident electrons is thus $\lambda \cong 83$ nm. Therefore, with such parameters we surely conclude that the transmission of the charge carriers shown in Fig. 3 [with $\xi = (E - \langle V \rangle)/E = -3$] is a purely propagating mode. As shown in this figure, the transmission of the electrons hitting to superlattice with large angles increases with increasing correlation between the random potentials of the barriers. In other words, applying correlation between the random potentials of the barriers causes to extend the angular window of the conducting mode around the normal incidence. This effect is in contrast with those results obtained with uncorrelated

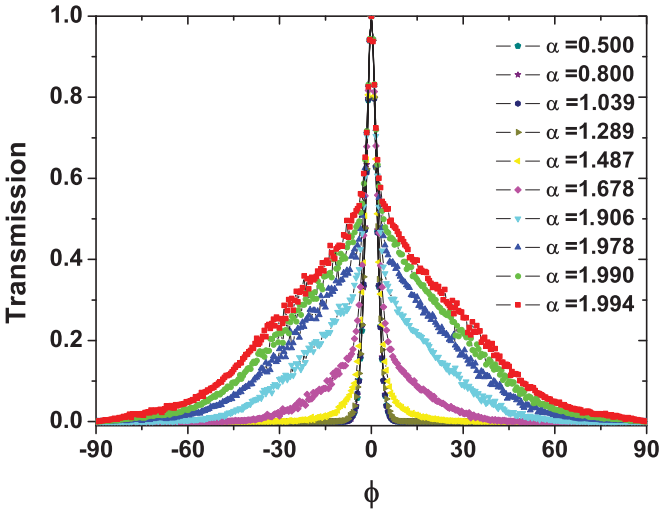

FIG. 3. (Color online) Transmission in terms of the incident angle hitting the graphene superlattice with various correlation exponents α. The number of the barriers is $N = 1000$. The averaged potential of the barriers and energy of the incident electrons are $\langle V \rangle = 200$ meV and $E = 50$ meV, respectively. Here, since $\xi = -3$, the transmission is calculated in the presence of purely propagating modes.

potentials of the barriers, in which the transmission of the massless carriers is suppressed for the wide range of the incident angles except $\phi = 0$. The perfect transmission at normal incidence can be described by the Klein tunneling. Similarly, in the correlated case, by increasing the disorder strength and also the number of the barriers, the transmission of the quasiparticles is suppressed at all values of the incident angle except at $\phi = 0$. Figure 4 shows the suppression of the transmission at large incident angles when the number of the potential barriers increases.

In the linear regime, the conductance is proportional to the angular-averaged transmission projected along the current direction. To understand how the correlation between random

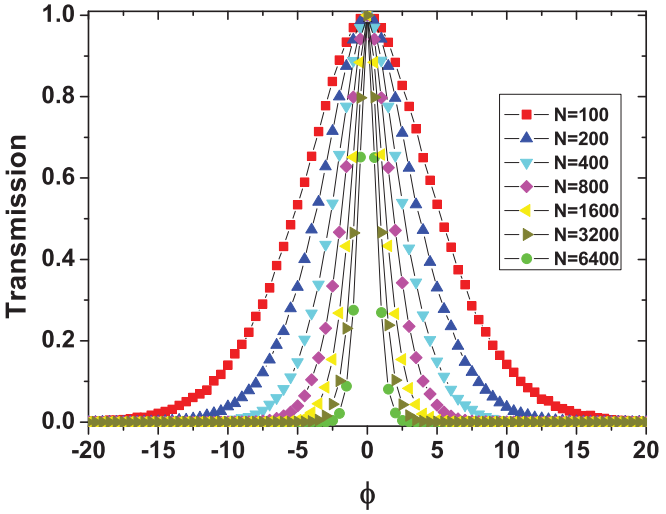

FIG. 4. (Color online) Transmission as a function of the incident angle through a graphene superlattice with long-range correlated random potentials for various barrier numbers N. Here $\alpha = 1.102$ and $\sigma = 0.1$.

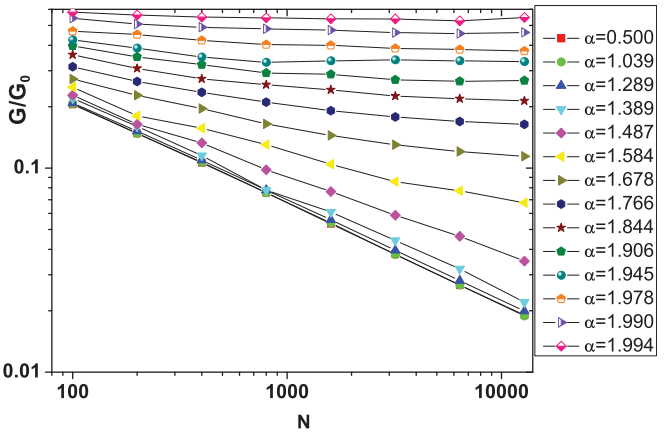

FIG. 5. (Color online) Conductance through a graphene superlattice with long-range correlated random potentials as a function of the barrier number N for $\sigma = 0.1$. This is finite-size scaling for different correlation exponents α. Here, $\langle V \rangle = 200$ meV and $E = 50$ meV.

potentials affects the transport properties of graphene superlattice, we calculate the size dependence of the conductance for various values of the correlation exponents; the results are plotted in Fig. 5. It is clear from the figure that there is a critical-correlation-exponent value of α such that for $\alpha < \alpha_{\rm cr}$, the conductance decreases with increasing system size, while it goes to a constant value for $\alpha > \alpha_{\rm cr}$. In other words, a consequence of applying long-range correlation is the emergence of a phase transition from the insulating to metallic states. It is worthwhile noting that this phase transition is not a finite-size effect. The conductance decreases with the number of the barriers with a power-law behavior. The following function is fitted to a log-log plot of the conductance:

$$\frac{G}{G_0} \propto N^{-\eta(\alpha,\sigma)}, \tag{13}$$

where η as a function of α and σ decreases, therefore, increasing the correlation exponent. Furthermore, the disorder strength strongly suppresses the conductance such that the critical correlation exponent, which means on the emergence of a phase transition, increases with the disorder strength.

The conductance through disordered potentials of barriers having correlation exponent $\alpha = 0.5$ decays with the barrier number as $N^{-0.5}$. The same decaying of the conductance was reported in Ref. 19 for a graphene superlattice with white-noise potentials distributed on the barriers. However, applying a long-range correlation between random potentials facilitates the conductance through the graphene superlattice.

A power-law fitting for the conductance is shown in Fig. 5. It has determined a dependency of η on the correlation exponent, α, and disorder strength, σ, which is represented in Fig. 6. For the sake of having the critical correlation exponent, we have used a transition function (such as the Fermi-Dirac function) as a fit function of the exponent function $\eta(\alpha,\sigma)$.

$$\eta(\alpha,\sigma) = \frac{\gamma}{e^{\beta(\alpha-\alpha_{\rm cr}(\sigma))}+1} \to \begin{cases} 0, & \alpha \gg \alpha_{\rm cr}, \\ \gamma, & \alpha \ll \alpha_{\rm cr}, \end{cases} \tag{14}$$

where β and $\alpha_{\rm cr}$ are fitted parameters and $\gamma = 0.5$ for $\xi = -3$. The interval at which $\eta(\alpha)$ decreases from the value of γ to zero is related with the inverse of β. The emergence of a transition

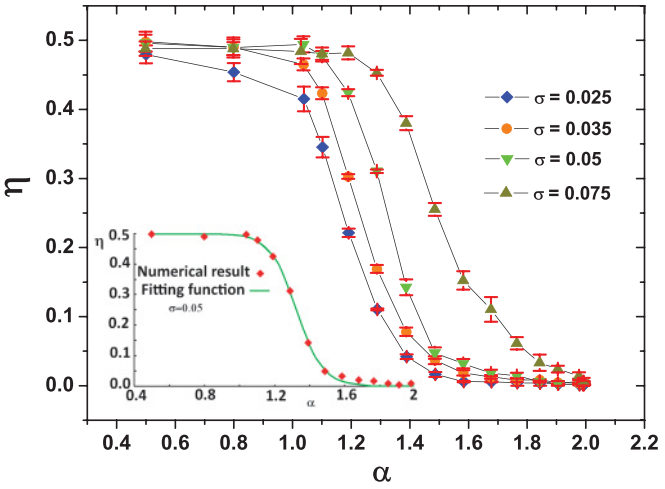

FIG. 6. (Color online) Exponent of the conductance in a power-law form $G/G_0 \propto N^{-\eta}$ as a function of correlation exponent α. In the inset, the fitting of a Fermi-Dirac-like function [Eq. (14)] to numerical data is shown.

from an insulating to a metallic phase corresponds to the variation of η from γ to 0. Now, we provide a phase-transition diagram in which the critical correlation exponent depends on the disorder strength. Figure 7 shows that the critical correlation exponent increases when the disorder strength increases up to $\sigma = 0.3$. Roughly speaking, the system remains in *a metallic phase* when the correlation is very long range at low disorder strength whereas it turns out to be an insulator at large disorder strength values and at midrange correlation. This phenomenon is robust against the type of disorder. In Appendix A, it is shown that instead of the barrier potentials, if disorder is distributed on the width of barriers, such transition from insulating to metallic phases still survives. Moreover, as shown in Appendix B, this phase transition is independent of the distribution function.

B. Energy range of the phase transition

To provide a fascinating experimental manifestation of the phase transition, it is significant to demonstrate that the phase

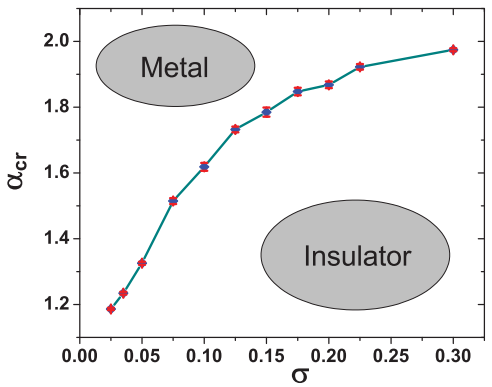

FIG. 7. (Color online) Metal-to-insulator phase diagram. The critical correlation exponent, α_{cr}, increases with the disorder strength, σ.

transition can exist in a continuum range of energies not just at some discrete energies.

Let us now concentrate on the conductance behavior in different ranges of the Fermi energy. For a single barrier on graphene, in the range of $-1 < \xi < 1$, it is proved that both the evanescent and propagating modes coexist.[33] Out of this range, all states are fully in the propagating mode. By considering this fact, we investigate the conductance as a function of ξ through a disordered graphene superlattice for several correlation exponent values and the results are shown in Fig. 8. It can be seen that the same behavior as for the single-barrier case appeared for different ranges of ξ. The contribution of the evanescent modes to the conductance is dominant in $\xi = 0$ and therefore the conductance is suppressed at this point. For $|\xi| \to 1$, the contribution of the propagating modes becomes dominant and thus the conductance increases

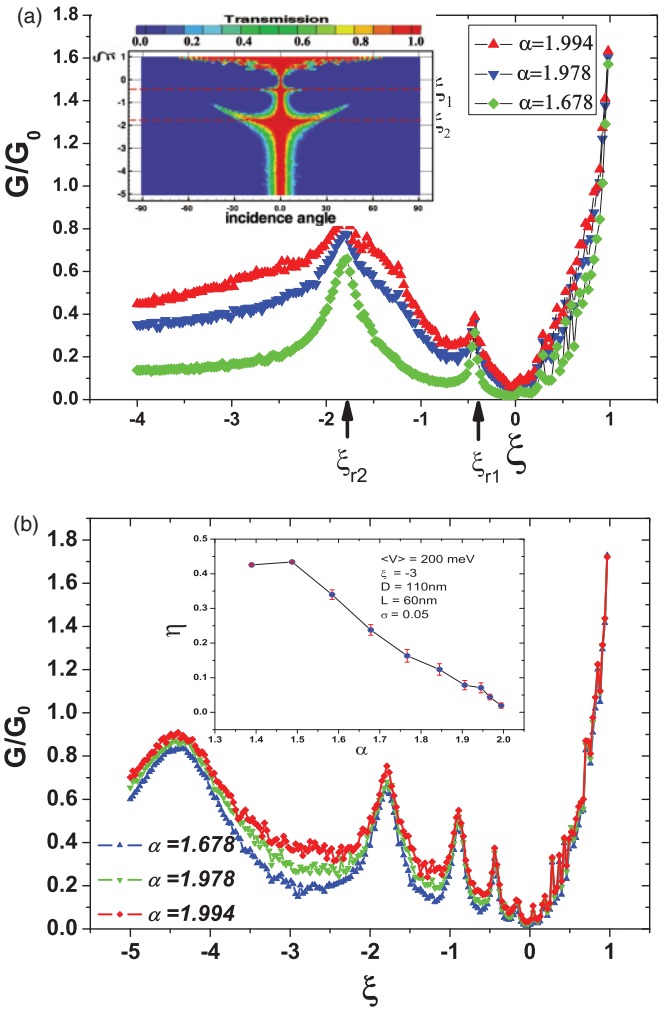

FIG. 8. (Color online) Functional of the conductance in terms of ξ that represents the Fermi energy for two structural parameters; (a) for $D = 50$ nm and $L = 30$ nm and (b) for $D = 110$ nm and $L = 60$ nm. The peaks in the conductance correspond to resonant states. Here $N = 800$ and $\sigma = 0.1$. The inset in (a) shows a 3D contour plot of the transmission in the plane of ξ and the incident angle. Resonant states correspond to a more angular-wide domain for transport. The inset in (b) demonstrates that the phase transition is robust against variation of the geometrical parameters.

continuously. For $\xi < 0$, the conductance oscillates at the resonant states that originate from the perfect tunneling of the charge carriers with nearly normal incidence. A 3D contour plot of the transmission in terms of ξ and the incident angle [see the inset of Fig. 8(a)] shows that at resonant states a conducting domain of the angles is opened around the normal incidence. The resonant condition for a single barrier in graphene is given by $k_F D\sqrt{\xi^2 - u^2} = n\pi$, where $u = \sin\varphi$. The energy separation of the resonant states can be extracted from expanding the resonant condition for normal incidence $u \ll \xi$. In this case, two sequential resonant states have a distance like $\Delta\xi_r \cong \frac{\pi}{k_F D}(1 - \frac{u^2}{2\xi^2})$. As a result, the period of the conductance is reduced with D and L while it is enhanced with $|\xi|$. A comparison between Figs. 8(a) and 8(b) demonstrates that by enlarging the structural parameters as nearly twice, the number of resonant peaks in the conductance subsequently doubles in a given ξ range. Furthermore, we can demonstrate that the phase transition is robust against the geometrical parameters. The inset in Fig. 8(b) shows the emergence of the phase transition for the values of $D = 110$ nm and $L = 60$ nm.

In the limit of $\xi \to 1$, which means $E \gg \langle V \rangle$, conducting channels are opened for the whole range of angles, $T(\phi) = 1$, and thus by using Eq. (12), we then get $\lim_{\xi\to 1} G/G_0 = 2$.

By applying a long-range correlation between the potentials of the barriers, we show in Fig. 8(a) that the conductance displays an enhancement in some ranges of the energy compared to the resonant states and the range including the evanescent modes, $|\xi| < 1$. To clarify this, firstly we investigate the conductance suppression with the number of the barriers in all ranges of the Fermi energy for a sequence of *white-noise disorder* distributed on the potentials of the barriers. The results are represented in Fig. 9(a), which shows a power-law form of the conductance in terms of the barrier numbers for different values of ξ. It is significant to understand

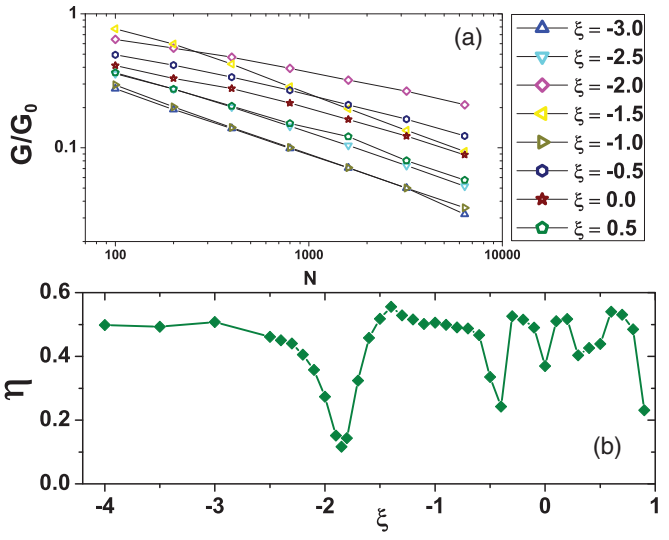

FIG. 9. (Color online) (a) Conductance in terms of the barrier numbers for graphene superlattice with *white-noise disorder* on potentials of the barriers and for different values of the Fermi level ξ. (b) Exponent of the conductance (η) in a power-law form $G/G_0 \propto N^{-\eta}$ as a function of ξ.

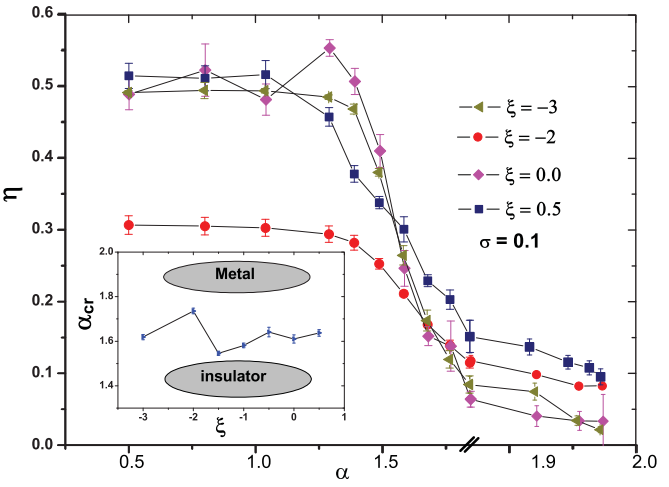

FIG. 10. (Color online) Exponent of the conductance in a power-law form $G/G_0 \propto N^{-\eta}$ as a function of the correlation exponent α for different values of ξ. In the inset the metal-to-insulator phase transition in all ranges of the energy.

how the exponent of η varies with the Fermi energy. The slope of the lines in the log-log plot of Fig. 9(a) for different ξ is indicated in Fig. 9(b). It is clear that close to the resonant states $\xi_r = -1.85$ and -0.45, the exponent of η reduces from the value of 0.5 to its resonant values $\eta_r = 0.12$ and 0.25, respectively. As a consequence, close to the resonant states the suppression of the conductance, which is induced by the random potentials of the barriers, is much weaker than for other states. The resonant value of η_r decreases when ξ goes away from the region that includes the evanescent modes $|\xi| < 1$.

Our numerical calculations demonstrate that the insulator-to-metal phase transition occurs in all ranges of the energy. It is clear from Fig. 10 that the phase transition appears not only at the propagating and resonant states, but also in the fully evanescent mode $\xi = 0$. In Fig. 10, η ($\alpha = 0.5$) decreases to 0.3 at $\xi = -2$, which is close to the second resonant state shown in Fig. 8(a). Another exception around the resonant states is the width of function $\eta(\alpha)$, which increases at the resonant states. Therefore, at the resonant states, the transition from an insulating to a metallic phase is smooth along the correlation exponent. The inset in Fig. 10 shows small fluctuations of the critical correlation exponent as a function of ξ. Accordingly, the phase transition is a general behavior for all ranges of the energy.

C. Resonance in the conductance

Now, we study the effect of the long-range correlated disorder on the resonance phenomena seen in the conductance. Resonance in the conductance of graphene superlattice with a white-noise disorder distributed on the width of the barriers has been studied before.[19] Figure 11 shows the conductance oscillations as a function of the barrier width (D) and also distance between barriers (L) for several values of the correlation exponent. Apparently, the application of the long-range correlation between the potentials of the barriers increases the conductance for all ranges of D and L. Moreover, as shown in Fig. 11(a), the conductance tends to a constant value after some oscillations in thin barriers independent of the barrier

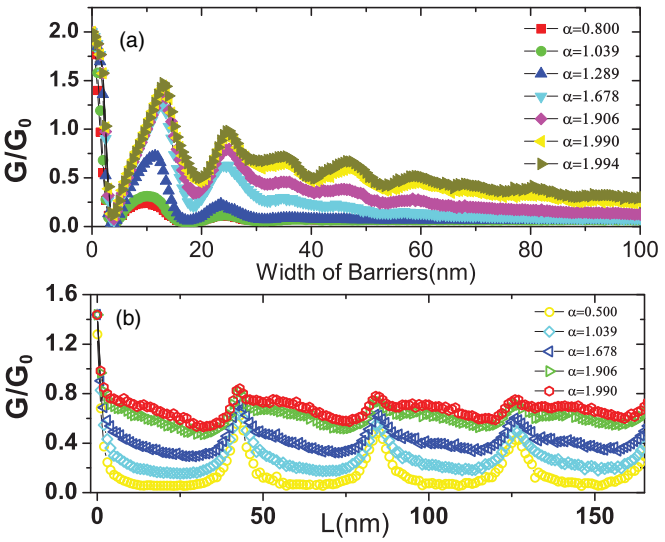

FIG. 11. (Color online) Conductance oscillations in terms of (a) the width (D) of the barriers (b) the distance (L) between barriers for different correlation exponents. Here $N = 800$ and $\sigma = 0.1$.

width. In fact, the transmission of the quasiparticles hitting the graphene superlattice at large incident angles is suppressed for the wide barriers, and thus only transmission arising from the Klein tunneling around the normal incidence contributes to the conductance integration given by Eq. (12). The same behavior occurs in the case of $N = 1$. The configuration average (C.A.) of the transmission through one barrier[34] depends on the width as $\langle \sin^2(k_x D)\rangle_{\text{C.A.}}$ and $\langle \cos^2(k_x D)\rangle_{\text{C.A.}}$, where k_x is a random parameter. It is trivial that the average of the transmission, and consequently of the conductance, are independent of the width if the D value increases. On the other hand, by applying the randomness on k_x, the resonant condition $k_x D = n\pi$ in wide barriers can not be satisfied, and thus there is no longer a resonant peak in the conductance.

Figure 11(b) shows the conductance oscillations as a function of L. In this case, the decaying of the oscillations is much weaker than the conductance oscillations with the barrier width. In fact, since there is no disorder in the wells, for a fixed barrier width, the resonant condition affects much less than the barrier resonant condition.

IV. CONCLUSIONS

By using the transfer matrix method, we investigated the conductance through a graphene superlattice with a long-range correlated disorder distributed on the potentials of the barriers. Applying a correlation between the potentials opens the angular-domain window of the conducting channels in competition with the factor of the disorder strength that suppress the transmission at large incident angles. As a result, the conductance increases with the correlation between the potentials of the barriers giving rise to a metallic phase. We obtain a phase transition diagram in which the critical correlation exponent for such a phase transition depends strongly on the disorder strength and slightly on the energy of the incident particles. At resonant states, the suppression of the conductance with the number of the barriers is much less than at other states. Last but not least, our finding for the dc conductance of the graphene superlattices should be important for the design of electronic nanodevices based on graphene superlattices.

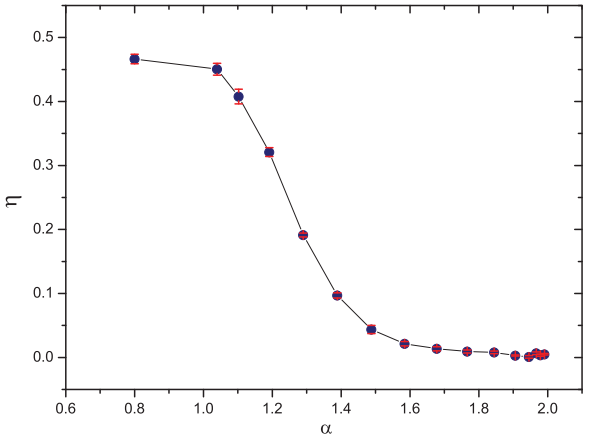

FIG. 12. (Color online) Emerging of the phase transition in a superlattice with *width fluctuations*. The exponent, η, of the conductance in a power-law form is $G/G_0 \propto N^{-\eta}$ and α is the correlation exponent.

APPENDIX A: PHASE TRANSITION IN THE PRESENCE OF WIDTH FLUCTUATIONS

It is worthwhile to examine the nature of the phase transition, in particular, whether it remains invariant under the application of fluctuations on the width of the barriers.[28,35] Though, from the experimental point of view, manufacturing a superlattice with disordered widths is less controllable than a superlattice with disordered heights.

To demonstrate robustness of the phase transition against width fluctuations, in the same way as we distributed disorder on the potentials, we define the width of the barriers to fluctuate around its mean as $D_i = \langle D\rangle(1 + \sigma\varepsilon_i)$. For this calculation, we assume that the energy of charge carriers and the averaged width of barriers is $E = 50$ meV and $\langle D\rangle = 50$ nm. The other

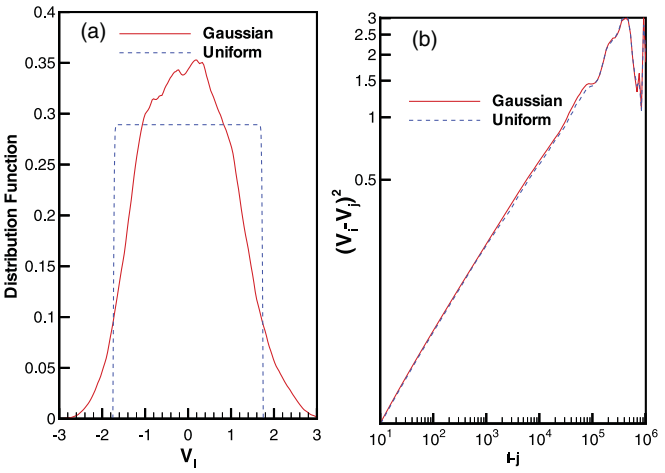

FIG. 13. (Color online) (a) Distribution function and (b) the pair correlation function of two random sequences with *uniform* and *Gaussian* distributions. The correlation exponent of these random sequences is $\alpha = 1.2$.

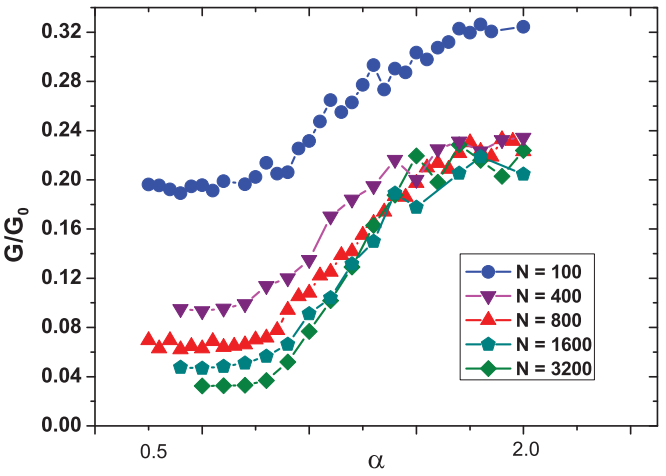

FIG. 14. (Color online) Conductance through a graphene superlattice with disordered potentials of barriers as a function of correlation exponent for different lengths. The distribution of randomness is *uniform*. Here, $E = 50$ meV, $\langle V \rangle = 200$ meV, and $\sigma = 0.1$.

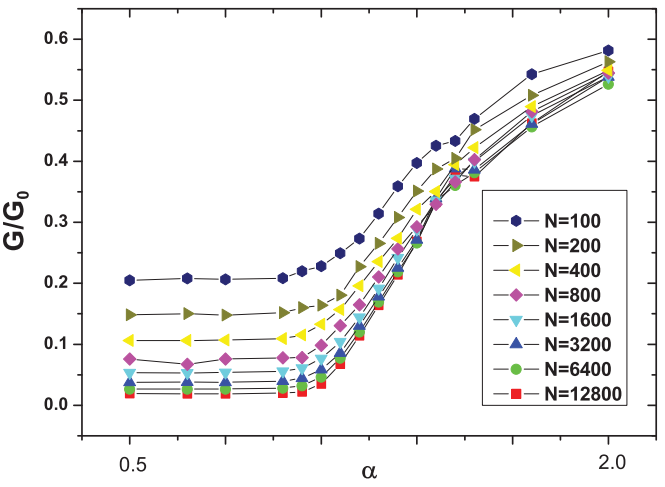

FIG. 15. (Color online) Conductance through a graphene superlattice with disordered potentials of barriers as a function of correlation exponent for different N and $\sigma = 0.1$. The distribution of potentials is *Gaussian*. Here, $E = 50$ meV and $\langle V \rangle = 200$ meV.

parameters are $V = 200$ meV, $\xi = -3$, $L = 30$ nm, and $\sigma = 0.05$. As it is seen in Fig. 12, the phase transition from the insulating to the metallic phase still survives when disorder is distributed on the width of barriers.

APPENDIX B: DISORDER DISTRIBUTION AND PHASE TRANSITION

We would like to show that the phase transition does not depend on the type of distribution function of correlated disorder. More precisely, the phase transition will be observed when the tails of the distribution function of disorder decay faster than a power-law form. As an example, we have reproduced the phase diagram of Fig. 6 but for a long-range correlated disorder with *uniform* distribution function. To do this, we have reproduced a correlated random sequence with uniform distribution by applying an algorithm on a correlated random sequence with Gaussian distribution. Figure 13 shows the distribution function and also the pair-correlation function of a generated random sequence with a uniform distribution that is compared with the correlated random sequence with a Gaussian distribution. The pair-correlation function is defined as

$$\langle [V_i - V_j]^2 \rangle_{\text{c.a.}} = 2\sigma^2 \left| \frac{i-j}{\ell_c} \right|^{2H} \qquad \text{(B1)}$$

where the correlation length (ℓ_C) is considered to be equal to the system size. Variables i and j are the positions of the barrier potentials along the superlattice. The Hurst exponent H is defined by $\alpha = 1 + H$. Figure 13(b) shows a log-log curve of the pair-correlation function as a function of $i - j$. The slope of the line in this figure determines H and also α.

By having such a random sequence, we calculate the conductance as a function of correlation exponent for different lengths. It is shown in Fig. 14 that in the thermodynamic limit and lower than a critical correlation exponent the conductance goes to zero by increasing the system length, while higher than the critical correlation exponent the conductance is robust against the system size and remains at a high value. Therefore, we can conclude that the phase transition also emerges for correlated disordered potentials of barriers with a uniform distribution.

Eventually, Fig. 15 shows the conductance as a function of correlation exponent for different N. It is seen that in the thermodynamics limit, higher than a critical correlation exponent, the conductance increases continuously, while lower than a critical value and for increased system length, the conductance goes to zero. By increasing N, the curves do not cut each other. Therefore, there is no discontinuity in the value of the conductance. It means that the phase transition is a *continuous-phase transition*. This phase transition is a transition from anomalously localized states[27,36] to extended states. Therefore, in the thermodynamic limit, there is a metal-to-insulator phase transition.

*cheraghchi@du.ac.ir
†asgari@ipm.ir

[1] K. S. Novoselov, A. K. Geim, S. V. Morozov, D. Jiang, Y. Zhang, S. V. Dubonos, I. V. Grigorieva, and A. A. Firsov, Science **306**, 666 (2004).
[2] A. Geim, Science **324**, 1530 (2009).
[3] R. Wallace, Phys. Rev. **71**, 622 (1947); T. Ando, J. Phys. Soc. Jpn. **74**, 777 (2005).
[4] V. P. Gusynin and S. G. Sharapov, Phys. Rev. Lett. **95**, 146801 (2005).
[5] X. Du, I. Skachko, F. Duerr, A. Luican, and E. Y. Andrei, Nature (London) **462**, 192 (2009); K. I. Bolotin, F. Ghahari, M. D. Shulman, H. L. Stormer, and P. Kim, *ibid.* **462**, 196 (2009).
[6] V. V. Cheianov, V. Falko, and B. L. Altshuler, Science **315**, 1252 (2007).
[7] C. W. J. Beenakker, Phys. Rev. Lett. **97**, 067007 (2006).

[8] A. Bostwick, F. Speck, T. Seyller, K. Horn, M. Polini, R. Asgari, A. H. MacDonald, and E. Rotenberg, Science **328**, 999 (2010).
[9] K. S. Novoselov, A. K. Geim, S. V. Morozov, D. Jiang, M. I. Katsnelson, I. V. Grigorieva, S. V. Dubonos, and A. A. Firsov, Nature (London) **438**, 197 (2005); Nat. Phys. **2**, 177 (2006).
[10] O. Klein, Z. Phys. **53**, 157165 (1929).
[11] J. R. Williams, L. DiCarlo, and C. M. Marcus, Science **317**, 638 (2007).
[12] N. Stander, B. Huard, and D. Goldhaber-Gordon, Phys. Rev. Lett. **102**, 026807 (2009).
[13] K. S. Novoselov, A. K. Geim, S. V. Morozov, D. Jiang, M. I. Katsnelson, I. V. Grigorieva, S. V. Dubonos, and A. A. Firsov, Nature (London) **438**, 197 (2005).
[14] Y. B. Zhang, Y. W. Tan, H. L. Stormer, and P. Kim, Nature (London) **438**, 201 (2005).
[15] J. Nilsson, A. H. Castro Neto, F. Guinea, and N. M. R. Peres, Phys. Rev. B **76**, 165416 (2007).
[16] H. Hiura, Appl. Surf. Sci. **222**, 374 (2004); J. C. Meyer, C. O. Girit, M. F. Crommie, and A. Zettl, Appl. Phys. Lett. **92**, 123110 (2008).
[17] B. Huard, J. A. Sulpizio, N. Stander, K. Todd, B. Yang, and D. Goldhaber-Gordon, Phys. Rev. Lett. **98**, 236803 (2007).
[18] C. Bai and X. Zhang, Phys. Rev. B **76**, 075430 (2007).
[19] N. Abedpour, Ayoub Esmailpour, Reza Asgari, and M. R. Tabar, Phys. Rev. B **79**, 165412 (2009).
[20] C.-H. Park, Y.-W. Son, L. Yang, M. L. Cohen, and S. G. Louie, Phys. Rev. Lett. **103**, 046808 (2009).
[21] L. Brey and H. A. Fertig, Phys. Rev. Lett. **103**, 046809 (2009).
[22] M. Barbier, P. Vasilopoulos, and F. M. Peeters, Phys. Rev. B **81**, 075438 (2010).
[23] K. Nomura and A. H. MacDonald, Phys. Rev. Lett. **98**, 076602 (2007); A. Rycerz, J. Tworzydlo, and C. W. J. Beenakker, Europhys. Lett. **79**, 57003 (2007); J. H. Bardarson, J. Tworzydlo, P. W. Brouwer, and C. W. J. Beenakker, Phys. Rev. Lett. **99**, 106801 (2007); K. Nomura, M. Koshino, and S. Ryu, *ibid*. **99**, 146806 (2007); P. San-Jose, E. Prada, and D. S. Golubev, Phys. Rev. B **76**, 195445 (2007).
[24] D. H. Dunlap, H. L. Wu, and P. W. Phillips, Phys. Rev. Lett. **65**, 88 (1990).
[25] V. Bellani, E. Diez, R. Hey, L. Toni, L. Tarricone, G. B. Parravicini, F. Dominguez-Adame, and R. Gomez-Alcala, Phys. Rev. Lett. **82**, 2159 (1999).
[26] F. A. B. F. deMoura and M. L. Lyra, Phys. Rev. Lett. **81**, 3735 (1998).
[27] H. Cheraghchi, S. M. Fazeli, and K. Esfarjani, Phys. Rev. B **72**, 174207 (2005).
[28] A. Esmailpour, M. Esmaeilzadeh, E. Faizabadi, P. Carpena, and M. R. Tabar, Phys. Rev. B **74**, 024206 (2006).
[29] U. Kuhl, F. M. Izrailev, A. A. Krokhin, and H.-J. Stöckmann, Appl. Phys. Lett. **77**, 633 (2000).
[30] Heinz-Otto Peitgen and Dietmar Saupe, *The Science of Fractal Images* (Springer-Verlag, New York, 1988).
[31] H. A. Makse, S. Havlin, M. Schwartz, and H. E. Stanley, Phys. Rev. E **53**, 5445 (1996).
[32] S. Datta, *Electronic Transport in Mesoscopic Systems* (Cambridge University Press, London, 1995).
[33] H. Haugen, D. Huertas-Hernando, and A. Brataas, Phys. Rev. B **77**, 115406 (2008).
[34] A. H. Castro Neto, F. Guinea, N. M. R. Peres, K. S. Novoselov, and A. K. Geim, Rev. Mod. Phys. **81**, 109 (2009).
[35] J. C. Hernandez-Herrejon, F. M. Izrailev, and L. Tessieri, e-print arXiv:1003.3691.
[36] G. Theodorou and M. H. Cohen, Phys. Rev. B **13**, 4597 (1976).